Alginate Hydrogel Microencapsulation Inhibits Devitrification and Enables Large-Volume Low-CPA Cell Vitrification

*Haishui Huang, Jung Kyu Choi, Wei Rao, Shuting Zhao, Pranay Agarwal, Gang Zhao, and Xiaoming He**

Cryopreservation of stem cells is important to meet their ever-increasing demand by the burgeoning cell-based medicine. The conventional slow freezing for stem cell cryopreservation suffers from inevitable cell injury associated with ice formation and the vitrification (i.e., no visible ice formation) approach is emerging as a new strategy for cell cryopreservation. A major challenge to cell vitrification is intracellular ice formation (IIF, a lethal event to cells) induced by devitrification (i.e., formation of visible ice in previously vitrified solution) during warming the vitrified cells at cryogenic temperature back to super-zero temperatures. Consequently, high and toxic concentrations of penetrating cryoprotectants (i.e., high CPAs, up to ≈8 M) and/or limited sample volumes (up to ≈2.5 µL) have been used to minimize IIF during vitrification. It is revealed that alginate hydrogel microencapsulation can effectively inhibit devitrification during warming. The data show that if ice formation were minimized during cooling, IIF is negligible in alginate hydrogel microencapsulated cells during the entire cooling and warming procedure of vitrification. This enables vitrification of pluripotent and multipotent stem cells with up to ≈4 times lower concentration of penetrating CPAs (up to 2 M, low CPA) in up to ≈100 times larger sample volume (up to ≈250 µL, large volume).

H. Huang, Dr. J. K. Choi, Dr. W. Rao, S. Zhao, P. Agarwal, Prof. X. He
Department of Biomedical Engineering
The Ohio State University
Columbus, OH 43210, USA
E-mail: he.429@osu.edu
H. Huang
Department of Mechanical Engineering
The Ohio State University
Columbus, OH 43210, USA
H. Huang, Dr. J. K. Choi, Dr. W. Rao, S. Zhao, P. Agarwal, Prof. X. He
Davis Heart and Lung Research Institute
The Ohio State University
Columbus, OH 43210, USA
Prof. G. Zhao
Center for Biomedical Engineering
Department of Electronic Science and Technology
University of Science and Technology of China
Hefei, Anhui 230027, P.R. China
Prof. X. He
Comprehensive Cancer Center
The Ohio State University
Columbus, OH 43210, USA

DOI: 10.1002/adfm.201503047

1. Introduction

With recent advances in cell-based medicine, the demand for living cells (particularly stem cells) is ever increasing.[1] Because continuous expansion of cells in vitro by culturing at 37 °C is expensive and time-consuming and may result in uncontrolled spontaneous differentiation of stem cells, banking living cells for future use by cryopreservation is an enabling technology to the eventual success of the burgeoning cell-based medicine.[2] Cell cryopreservation is achieved by first cooling cells to usually below −80 °C so that all the biophysical and biochemical activities in cells are arrested (i.e., the cells enter a state of suspended animation), followed by warming back for use at a desired future time.[3]

Intracellular ice formation (IIF) has been recognized as a lethal event to cells during cell cryopreservation.[4] Two conventional approaches have been commonly adopted to minimize IIF: slow freezing and conventional high-cryoprotectants (CPAs) vitrification. For the former, cells are gradually dehydrated due to exosmosis driven by the elevated osmolality of extracellular solution when extracellular water transforms into ice during freezing at a slow cooling rate (typically less than 5 °C min^{-1}), which is referred as freeze concentration and can cause significant damage to cells.[2b,5] On the other hand, conventional high-CPA vitrification is achieved by using penetrating CPAs such as dimethylsulfoxide (DMSO) and 1,2-propanediol (PROH) at concentrations that are much higher than that used for slow freezing (up to 8 M vs ≈1–2 M), which is toxic to cells due to the high CPA-induced metabolic and osmotic (including cell dehydration) injuries.[6] As a result, multiple steps are required to gradually load (before cooling) and unload (after warming) the CPAs to potentially reduce the high-CPA cytotoxicity, which is time-consuming and stressful.[4b,7] To overcome these problems, low-CPA vitrification has been explored for cell cryopreservation by using various methods and devices such as electron microscopy grid and quartz microcapillary (QMC)[2a,4b,7d,8] to achieve ultra-rapid cooling rates that minimize IIF by reducing the time available for ice nucleation and growth. Although the cooling rates can be

very high (up to ≈10^6 °C min^{-1}) to achieve vitrification (defined as no visible ice formation in this study in accordance with the literature[9]) by plunging the devices into liquid nitrogen due to the boiling of liquid nitrogen, the warming rate by plunging the devices into an aqueous solution is usually much lower.[10] Consequently, IIF induced by devitrification during warming has been a major challenge to achieve high cell survival post vitrification.[11] Furthermore, the sample volume is limited to several microliters in these low-CPA vitrification devices for obtaining a high surface area to volume ratio to enhance cooling and warming during vitrification.[4b,7d,8d,e]

More recently, microencapsulation of living cells in hydrogel has been explored as a potential strategy to enhance cell cryopreservation mainly by slow freezing. For example, it was found that microencapsulation of human embryonic stem cells or spheres of mouse neuroblastoma cells in alginate hydrogel improves their post-cryopreservation survival by slow freezing.[12] However, microencapsulation of porcine and ovine mesenchymal stromal cells in polyethylene glycol (PEG) hydrogel microcapsules does not affect their survival post cryopreservation by slow freezing.[13] Moreover, it has been reported that the DMSO concentration could be reduced to 1.5 M for vitrification in QMC (≈2.5 µL sample volume) if mouse mesenchymal stem cells were microencapsulated in alginate hydrogel, which is partially attributed to the preferential vitrification of water in alginate hydrogel microcapsule compared to the water in the bulk solution outside the microcapsule during cooling.[8d] However, such vitrification study has not been performed for the more stress-sensitive embryonic stem cells (ESCs) and adult human stem cells, particularly in a large sample volume for the practical application to bank stem cells. Moreover, the mechanism by which the alginate hydrogel microencapsulation protects cells from IIF during the warming phase of vitrification has not been investigated.

Here, we report low-CPA vitrification of mouse embryonic stem cells (mESCs) and human adipose–derived stem cells (hADSCs) using conventional plastic straw (PS that was believed and used for conventional high-CPA vitrification only) by microencapsulating the cells in alginate hydrogel. Cell microencapsulation was performed using a nonplanar microfluidic device. IIF in the cells during both the cooling and warming stages of vitrification was studied using cryomicroscopy. It was found that significant IIF could occur during the warming phase of vitrification, which could be effectively inhibited by alginate hydrogel microencapsulation. Ultimately, the microencapsulated cells could be vitrified in QMC and PS with high post-cryopreservation viability and intact function using only 1.5 M (for QMC with up to ≈2.5 µL in sample volume) or 2 M (for PS with up to ≈250 µL in sample volume) penetrating CPA (PROH). The capability of achieving low-CPA (2 M) vitrification using PS for a large sample volume (≈250 µL) resolves all the challenges associated with existing cryopreservation technologies including low-CPA vitrification using QMC that is limited to a small (<≈2.5 µL in each QMC) sample volume, conventional high-CPA vitrification requiring a highly cytotoxic concentration (up to ≈8 M) of penetrating CPA, and conventional slow-freezing with inevitable freezing-induced cell injury. Therefore, alginate hydrogel microencapsulation holds great promise to enhance vitrification for banking living cells to meet their ever-increasing demands by the burgeoning cell-based medicine.

2. Results

2.1. Microfluidic Production of Cell-Laden Alginate Hydrogel Microcapsules

As shown in **Figure 1** (inset i) and Movie S1 (Supporting Information), at the microfluidic flow-focusing junction, the aqueous core (from inlet I1) and shell (from inlet I2) fluids (aqueous alginate solution) are dispersed into microdroplets in the continuous flow of oil emulsion (aqueous solution of calcium chloride emulsified in mineral oil from inlet I3) as a result of the Rayleigh–Plateau instability.[14] The core fluid may contain mESCs or hADSCs. The shell fluid is arranged to surround the core fluid in the microchannels entering the flow-focusing junction both horizontally and vertically (Figure S1A, Supporting Information). Under the flow conditions of this study, the microdroplet formation process falls into dripping mode and the microdroplet size is highly monodisperse (Move S1, Supporting Information).[15] After flow focusing, the aqueous microdroplets are gelled into hydrogel microcapsules in the downstream microchannel because the sodium alginate in the microdroplets

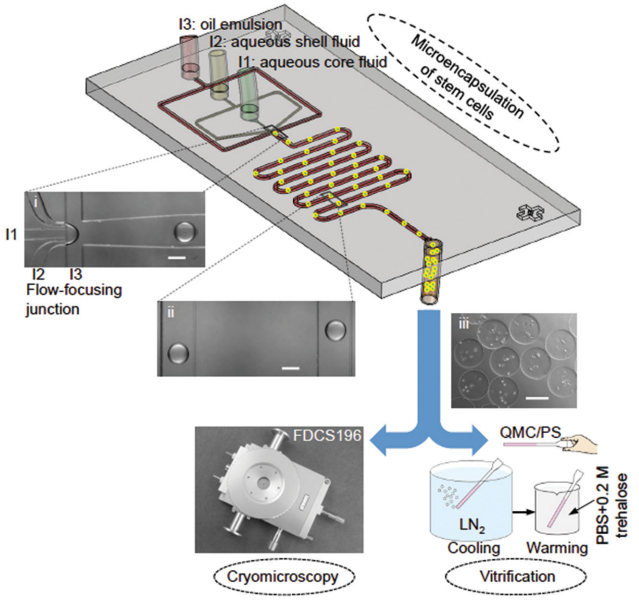

Figure 1. A schematic illustration of the experimental setup and procedure. The procedure includes three major steps: microencapsulation of murine embryonic stem cells (mESCs) or human adipose–derived stem cells (hADSCs) using a nonplanar microfluidic flow-focusing device, cryomicroscopy study of inhibiting devitrification and intracellular ice formation (IIF) using a Linkam cryostage, and vitrification study of cell survival and function with quartz microcapillary (QMC) and conventional plastic straw (PS). The insets (i), (ii), and (iii) are typical images of microdroplets at the proximal of the flow-focusing junction, alginate hydrogel microcapsules in the serpentine channel, and collected stem cell–laden microcapsules, respectively. The microcapsules are highly monodisperse (≈220 µm) as the droplet pinching-off falls into the dripping mode of flow instability. LN_2: liquid nitrogen. PBS: phosphate buffered saline (isotonic by default). Scale bars: 200 µm.

can be cross-linked into hydrogel of calcium alginate by Ca^{2+} in the continuous flow of oil emulsion.[16] Since the Reynolds number (Re) is far less than 1 (≈0.01), the movement of the dispersed/suspended alginate microcapsules is dominated by viscous force.[16a] As a result, the microdroplets or microcapsules travel along the central streamline in the microchannel (inset ii in Figure 1).[17] The cell-laden microcapsules produced by this method are spherical with a diameter of ≈220 µm (inset iii in Figure 1). Due to the presence of the shell fluid, most of the cells are confined in the interior of the resultant microcapsules to ensure high viability (>90%) by minimizing their contact with the surrounding oil. The encapsulated cells were used for further cryomicroscopy and vitrification studies to understand IIF during both cooling and warming and its correlation to the cell survival and functions including stemness and guided differentiation after vitrification.

2.2. Cryomicroscopy Study of IIF in Stem Cells during Low-CPA Vitrification

The cumulative percentage of mESCs with IIF during both the cooling and warming stage of vitrification under five different conditions are shown in **Figure 2**A. The corresponding representative phase images are given in Figure 2B where IIF shows up as darkening in the cells likely due to the precipitation of intracellular solutes when intracellular water forms ice. For mESCs without (W/O) encapsulation (Encap) and W/O CPA, ice forms first in the extracellular solution at ≈–21 °C, which triggers IIF in ≈12.5% of the mESCs instantaneously (within 0.4 s) (Figure 2A).[6a,18] However, IIF does not occur in more cells during further cooling to –60 °C. More importantly, IIF starts to occur again at ≈–13 °C and forms in all mESCs at ≈–7 °C during warming, probably due to the growth of extracellular ice.[8a,11b,d,e] Interestingly, the presence of low concentration of CPA (W/CPA, that is, the combination of 1.5 M PROH and 0.5 M trehalose as the penetrating and nonpenetrating CPAs, respectively) increases the occurrence of IIF in mESCs to ≈30% during cooling although it delays the first occurrence of IIF to a slightly lower temperature (–22 °C). During warming, the presence of low CPA advances the first occurrence of IIF to an earlier time or lower temperature (≈–22 °C) and IIF forms in all mESCs at ≈–15 °C, again probably due to the growth of extracellular ice.

If mESCs are microencapsulated in alginate hydrogel microcapsule, IIF starts at a slightly higher subzero temperature (≈–17 °C) W/O CPA and forms in all mESCs at ≈–23 °C during cooling. The presence of low CPA shifts the starting and ending temperatures of IIF during cooling to ≈–22 and –30 °C, respectively. In addition, the alginate microcapsules become wrinkled post cooling and warming without any CPA while they stay intact after the same procedure in the presence of low CPA (Figure 2B). This could be explained by the preferential vitrification of water in alginate hydrogel microcapsules in the presence of low CPA.[8d] In other words, the hydrogel network in the microcapsules can be mechanically deformed by the extensive ice formation during cooling and warming without CPA, which causes irreversible damage to the microcapsules after warming back to room temperature. Similar results of IIF and change in the morphology of microcapsules were observed from cryomicroscopy studies of hADSCs (Figure S2, Supporting Information).

More importantly, if the medium outside the cell-laden microcapsule is replaced with mineral oil, no ice formation is visible in the microcapsule and no IIF is observable in the microencapsulated cells throughout the entire cooling and warming procedure (last row in Figure 2B and Figure S2, Supporting Information, for mESCs and hADSCs, respectively).

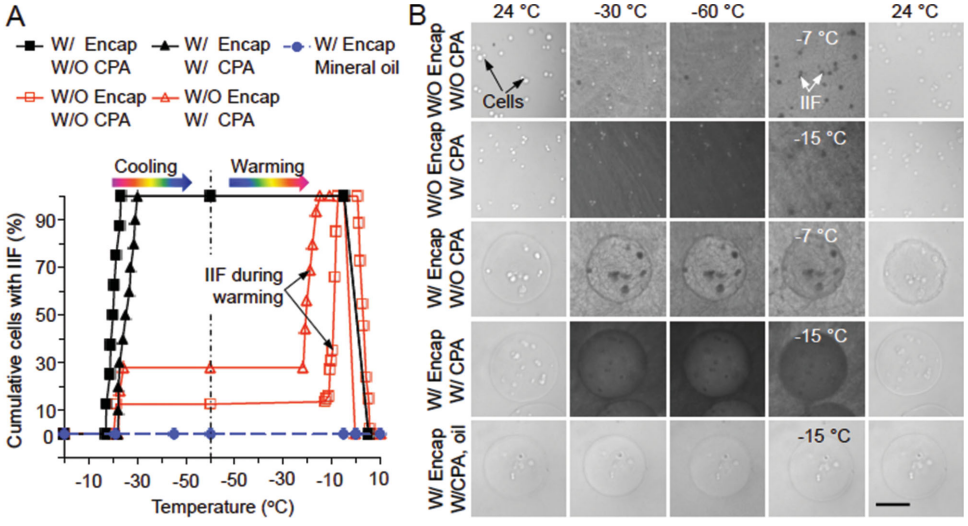

Figure 2. Intracellular ice formation (IIF) in mESCs from cryomicroscopy studies. A) The cumulative percentage of cells with IIF under five different conditions: (1) without (W/O) encapsulation (Encap) and W/O cryoprotectant (CPA), (2) W/O Encap and with (W/) CPA, (3) W/Encap and W/O CPA, (4) W/Encap and W/ CPA in culture medium, and (5) W/Encap and W/CPA in mineral oil. The CPA is a combination of 1.5 M 1,2-propanediol (PROH, penetrating) and 0.5 M trehalose (nonpenetrating). Both the cooling and warming rates are 60 °C min^{-1}. B) Typical images of mESCs during cooling and warming under the same five conditions in (A). The cells with and without IIF can be identified by the dark and bright spots, respectively. Scale bar: 100 µm.

These observations suggest that if the microencapsulated cells are cooled in aqueous solutions (rows 3–4 of Figure 2B and Figure S2, Supporting Information), ice crystals initiate in the aqueous solution outside the microcapsule and then propagate into the microcapsule to trigger IIF in the microencapsulated cells. However, it is extremely difficult (if not impossible) to achieve vitrification of the bulk aqueous solution outside the microcapsules during cooling with this low concentration of CPA using the cryomicroscopy system to test this hypothesis. This is because the highest cooling rate that can be achieved with the cryomicroscopy system is no more than 100 °C min^{-1}. Therefore, we conducted vitrification study using QMC and PS to overcome this problem.

2.3. Low-CPA Vitrification of Microencapsulated Cells Using QMC

Due to its miniaturized diameter and wall thickness (Figure S1B, Supporting Information), QMC can be used to create an ultrafast cooling rate by plunging it into liquid nitrogen to minimize ice formation in the small volume (up to 2.5 µL) of sample contained in it.[7d] As shown in **Figure 3**A and Movie S2 (Supporting Information), the vitrification solution for QMC (VSQ: cell culture medium containing 1.5 M PROH and 0.5 M trehalose as the penetrating and nonpenetrating CPAs, respectively) stays clear while the cell culture medium without any CPA appears opaque (or whitish) after plunging into liquid nitrogen, suggesting that VSQ was successfully vitrified with no visible ice formation while extensive ice formed in the medium without any CPA. Therefore, we performed further study to examine the viability of mESCs and hADSCs post vitrification in the VSQ using QMC both with and without microencapsulation. As shown in Figure 3B,C and Figure S3 (Supporting Information), most of the microencapsulated mESCs and hADSCs can survive the vitrification procedure. In stark contrast, nearly all mESCs and hADSCs without microencapsulation are dead (cell viability of the nonencapsulated mESCs and hADSCs is ≈0.4% and 3.5%, respectively) after vitrification using the same procedure for vitrifying the microencapsulated cells with QMC and VSQ.

These results indicate that the significant IIF (a lethal event to living cells) in the microencapsulated mESCs and hADSCs observed during cooling at a slow cooling rate (60 °C min^{-1}) with the cryomicroscopy system (Figure 2 and Figure S2, Supporting Information) can be effectively eliminated by using the VSQ and QMC for vitrification to create an ultrafast cooling rate and minimize ice formation in the bulk solution outside the microcapsules during cooling (Figure 3A and Movie S2, Supporting Information). This supports the aforementioned hypothesis that IIF in the microencapsulated cells during cooling is triggered by ice formation in the bulk aqueous solution outside the microcapsules. Moreover, the fact that nearly all of the nonencapsulated cells die post vitrification using QMC and VSQ suggests that devitrification of the previously (i.e., during cooling) vitrified bulk extracellular solution occurs and induces significant IIF during warming when using the QMC and VSQ for vitrification. Furthermore, this supports the hypothesis that alginate hydrogel microencapsulation

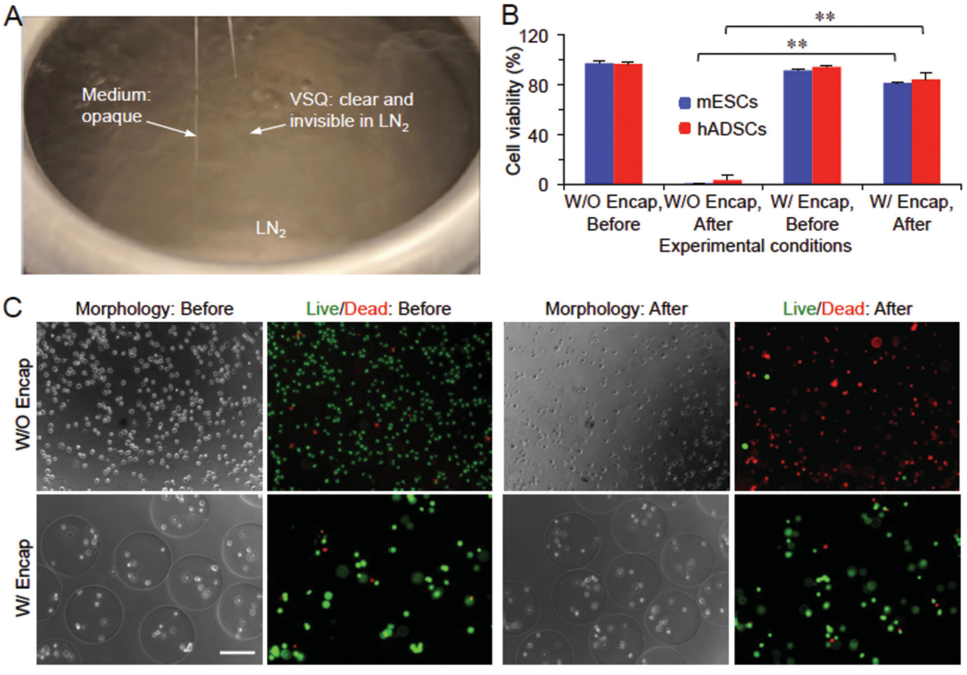

Figure 3. Low-CPA vitrification of stem cells using quartz microcapillary (QMC). A) A typical picture showing vitrification (clear appearance or no visible ice formation) of VSQ but not medium in QMC by plunging the QMC into liquid nitrogen (LN_2) for cooling. VSQ: Vitrification solution for QMC which is mESC or hADSC medium with 1.5 M 1,2-propanediol (PROH, penetrating) and 0.5 M trehalose (nonpenetrating). The QMC with an opaque appearance on the left is filled with cell culture medium without any CPA. B) Viability of mESCs and hADSCs either with (W/) or without (W/O) alginate hydrogel encapsulation (Encap) before and after vitrification in VSQ. **: $p < 0.01$. C) Typical phase and fluorescence images showing the viability of mESCs before and after vitrification in VSQ. Scale bar: 200 µm.

could effectively inhibit devitrification to minimize IIF during warming in view of the high viability of the microencapsulated mESCs and hADSCs shown in Figure 3B,C and Figure S3 (Supporting Information). However, devitrification of the bulk VSQ in QMC during warming is difficult to visualize because of the high rate and short time for warming. Therefore, we further performed vitrification studies using PS to test the hypothesis on the exceptional capability of inhibiting devitrification to minimize IIF during warming by alginate hydrogel microencapsulation.

2.4. Low-CPA Vitrification of Microencapsulated Cells Using PS

With a maximum sample volume of ≈100 times more than QMC (Figure S1B, Supporting Information), the PS has been widely used for cell cryopreservation by both slow freezing with a low concentration (1–2 M) of CPA and conventional high-CPA vitrification with a high and toxic concentration (up to 8 M) of penetrating CPA. However, it has never been used for low-CPA vitrification. Because of its large sample volume and large size compared to the QMC (Figure S1B, Supporting Information), the VSQ that is good for vitrification in QMC does not work for PS (**Figure 4**A). Therefore, we developed the vitrification solution for PS (VSP: cell culture medium containing 2 M PROH and 1.3 M trehalose as the penetrating and nonpenetrating CPAs, respectively) that can be vitrified without visible ice formation in the bulk solution by plunging the PS into liquid nitrogen for cooling (Figure 4A). Moreover, extensive ice formation in the bulk VSP is visible (whitish opaque) during warming (Figure 4A and Movie S3, Supporting Information), indicating devitrification does occur in the bulk VSP during warming.

The quantitative and qualitative data of cell viability of mESCs and hADSCs post vitrification using the PS together with VSP are shown in Figure 4B and Figure S4 (Supporting Information), respectively. These data are similar to that obtained using QMC and VSQ for the two types of stem cells: most of the microencapsulated cells could survive while almost all nonencapsulated cells are killed during the vitrification procedure. They demonstrate that IIF induced by devitrification during warming kills most nonencapsulated cells and alginate hydrogel microencapsulation can effectively protect the encapsulated cells by inhibiting devitrification to minimize IIF. We have performed this experiment for many times (>10) and the results are consistent. However, the survived cells must be capable of functioning normally in order to ascertain the effectiveness of our low-CPA (2 M penetrating CPA) vitrification approach with the PS developed in this study. Therefore, further studies were performed to examine the functional properties including stemness and capability of guided (or directed or coaxed) differentiation of the mESCs and hADSCs before and after the low-CPA vitrification with PS.

2.5. Functional Properties of mESCs and hADSCs Post Low-CPA Vitrification with PS

The functional properties for mESCs before and after the low-CPA vitrification with PS are shown in **Figure 5**. At the level of gene expression determined by quantitative real-time polymerase chain reaction (qRT-PCR), no significant difference is observed for the expression of four typical stem cell genes (Nanog, Sox2, Klf2, and Oct4) between the encapsulated mESCs post vitrification and the cells before vitrification either with or without encapsulation (Figure 5A). At the level of protein expression, the undifferentiated properties of the pluripotent mESCs after vitrification are not compromised as indicated by the staining of transcription factor Oct4 and membrane surface glycoprotein SSEA-1 (Figure 5B). The expressions of these protein makers, determined by flow cytometry, among the three different groups of mESCs are also not significantly different (Figure 5C). To determine the capability of differentiation of mESCs post vitrification, they were guided toward the cardiac lineage by using a combination of BMP-4 and bFGF.[19] The results demonstrate that mESCs in all the three groups could beat spontaneously after differentiation and there is no significant difference among these groups in terms of the percentage of beating foci (Figure 5D). Finally, immunofluorescence and flow cytometry studies were conducted to examine the protein expression of cTnT, a protein marker specific for cardiomyocytes. As shown in Figure 5E, there is positive staining of cTnT for the cells differentiated from the mESCs in all the three different groups. Furthermore, the difference in mean intensity of cTnT staining is minimal between the three different groups (Figure 5F).

The functional properties for hADSCs before and after the low-CPA vitrification with PS are shown in **Figure 6**. The expressions of stem cell genes (Nanog, Oct4, Sox2, and Klf4) of encapsulated hADSCs post vitrification are not significantly different from that of nonvitrified cells either with or without microencapsulation (Figure 6A). Immunostaining study was conducted to examine the expression of CD44 and CD31. The former is a common surface glycoprotein/receptor highly expressed on hADSCs

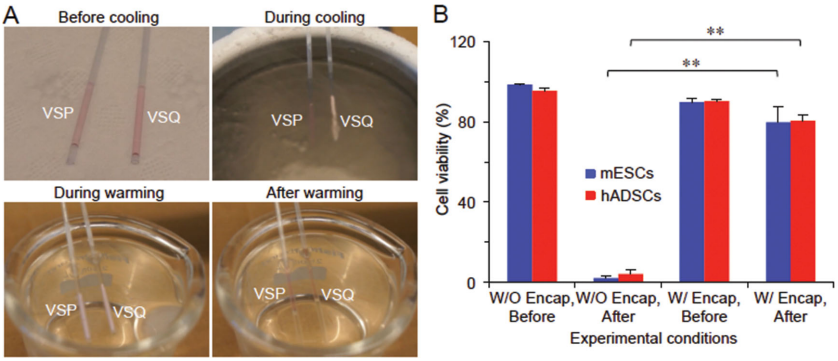

Figure 4. Low-CPA vitrification of stem cells with conventional plastic straw (PS). A) Typical images showing the vitrification of VSP but not VSQ during cooling with PS and devitrification of the vitrified VSP during warming with the PS. VSP: Vitrification solution for PS which is the culture medium of mESCs or hADSCs with 2 M PROH (penetrating) and 1.3 M trehalose (nonpenetrating). B) Viability of mESCs and hADSCs either with (w/) or without (W/O) alginate hydrogel encapsulation (Encap) before and after vitrification in VSP. **: $p < 0.01$.

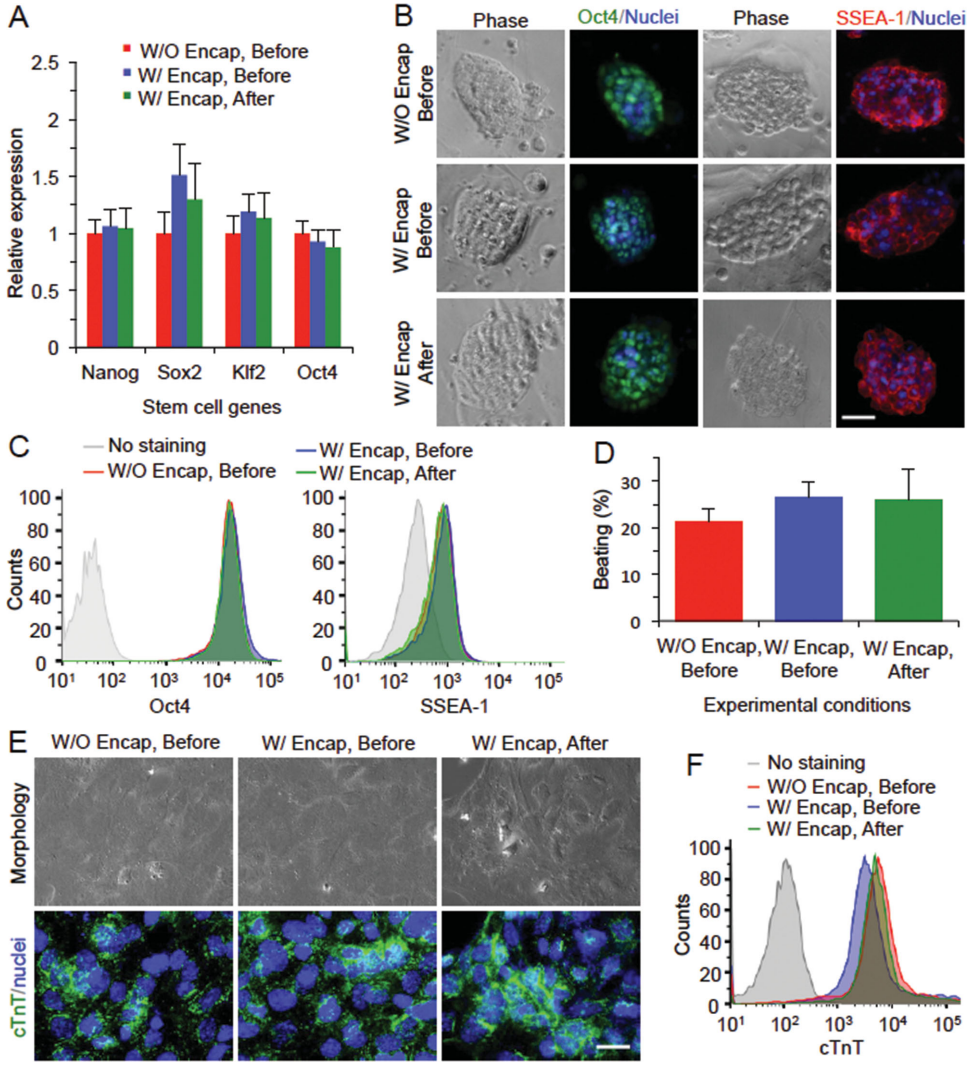

Figure 5. Intact stemness and function of mESCs after low-CPA vitrification in VSP with PS. A) Relative expressions of four stem cell genes determined by quantitative RT-PCR. B) Immunostaining of stem cell protein markers including stage specific embryonic antigen 1 (SSEA-1) and Oct4. C) Quantitative data of Oct4 and SSEA-1 staining from flow cytometry. D) The percentage of beating foci after mESCs are guided toward cardiac lineage. E) Immunostaining of cardiac troponin T (cTnT) as the specific marker of cardiomyocytes along with nuclei staining and images of the cell morphology. F) Flow cytometry data of cTnT staining. Scale bars: 50 μm in (B) and 20 μm in (E). No significant difference was observed between the mESCs before and after vitrification either with (W/) or without (W/O) encapsulation (Encap).

while the latter is a negative marker for the hADSCs. As shown in Figure 6B, low-CPA vitrification in VSP using PS and alginate hydrogel microencapsulation does not appear to have significant impact on the expression of the two receptors on the hADSCs. Moreover, the expression of the two surface markers on the hADSCs was studied quantitatively by flow cytometry and the results show that the expression of the positive marker CD44 on the vitrified hADSCs is similar to that on the non-cooled control cells, while the expression of negative surface marker CD31 is low in hADSCs for all the three different groups (Figure 6C). The stemness of the hADSCs was further tested by their capability of guided adipogenic, osteogenic, and chondrogenic differentiation and the results are shown in Figure 6D. For adipogenic differentiation, three weeks after initial induction, we observed Oil red O (ORO) staining of lipid droplets in the differentiated cells in all the three groups. For osteogenic differentiation, all the cells maintain similar osteogenic potential based on Alizarin red S (ARS) staining of calcific deposition. For chondrogenic differentiation, Alcian blue (AB) staining of sulfated proteoglycan deposits indicative of the presence of functional chondrocytes is observable in all the three groups. Moreover, quantitative analyses of the three different stains indicate neither microencapsulation nor vitrification has significant impact on the capability of adipogenic, osteogenic, and chondrogenic differentiation of the hADSCs (Figure 6D).

Collectively, the data of stemness and guided differentiation at the levels of both gene and protein expression shown in Figures 5 and 6 demonstrate that low-CPA vitrification using PS does not compromise the specific functional properties of both mESCs and hADSCs, which indicates that alginate hydrogel microencapsulation could effectively protect the encapsulated cells from cryoinjury during warming by inhibiting devitrification.

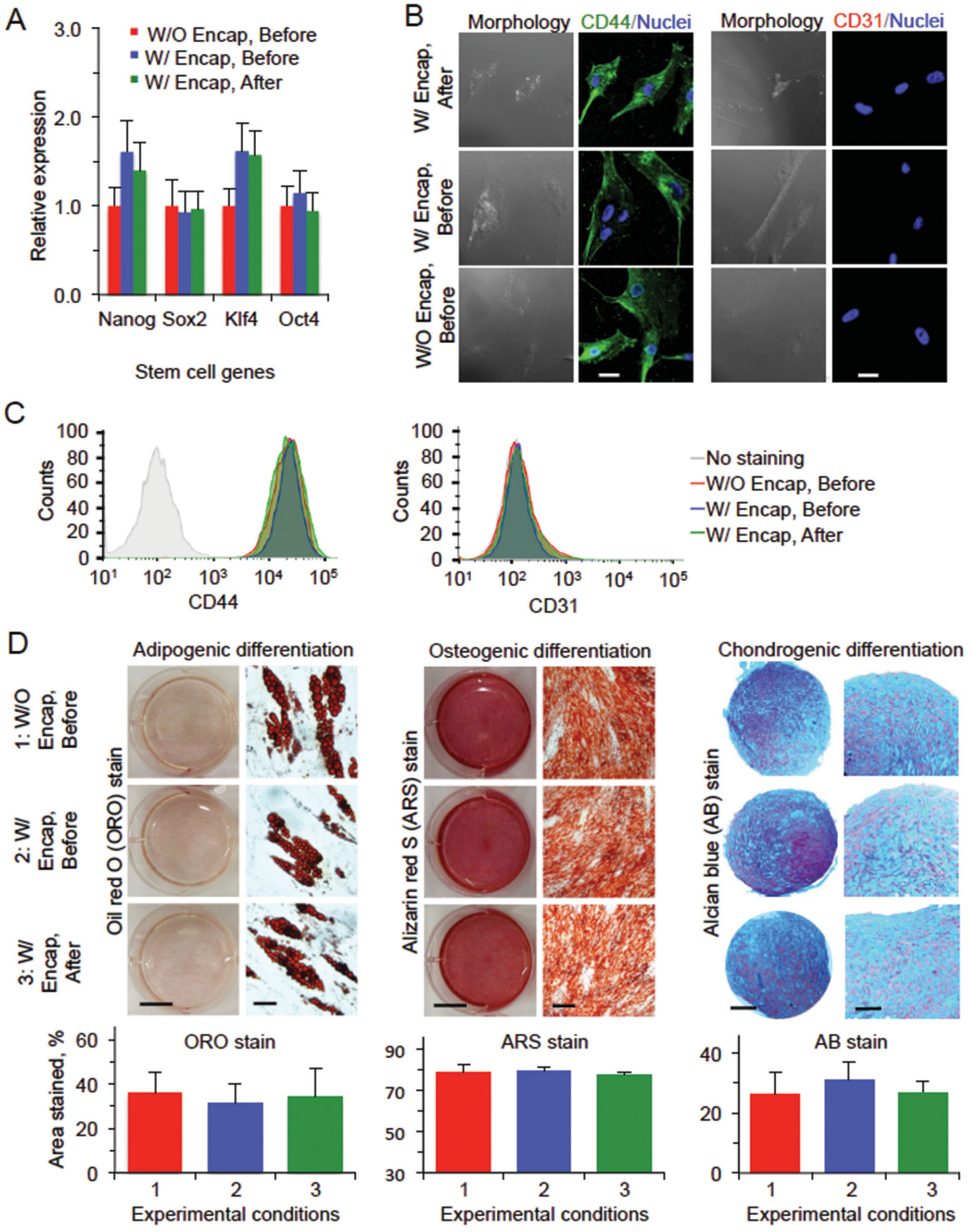

Figure 6. Intact stemness and function of hADSCs after low-CPA vitrification in VSP with PS. A) Relative expression of four stem cell genes determined by quantitative RT-PCR. B) Immunostaining of CD44(+) and CD31(–) showing the expression of the two markers on the cells. C) Quantification of CD44(+) and CD31(–) expression on the cells by flow cytometry. D) Qualitative and quantitative data on adipogenic, osteogenic, and chondrogenic differentiations of hADSCs. Scale bars: 25 μm in (B), 10 mm (left) and 40 μm (right) for adipogenic differentiation in (D), 10 mm (left) and 200 μm (right) for osteogenic differentiation in (D), and 200 μm (left) and 100 μm (right) for chondrogenic differentiation in (D). No significant difference was observed between the hADSCs before and after vitrification either with (W/) or without (W/O) encapsulation (Encap).

2.6. Cryomicroscopy Study of Inhibiting Devitrification by Alginate Hydrogel Microencapsulation

We further investigated the capacity of inhibiting devitrification by alginate hydrogel microencapsulation using cryomicroscopy. **Figure 7** shows the size and morphology of visible ice crystals outside the alginate hydrogel microcapsule in the bulk solution, at –60 °C (at the end of cooling) and at –7 or –15 °C (during warming) of mESC medium either without (Figure 7A) or with (Figure 7B) CPA (1.5 M PROH and 0.5 M trehalose) under phase (grayscale) and polarized (color) light microscopy. The blue and pink regions in the polarized microscopy images indicate ice crystals of different crystallographic orientations. For medium without CPA, fine ice crystals (FICs, single asterisk) suddenly form around –20 °C (Figure 2) during cooling and do not change much with further cooling to –60 °C. During warming, however, the FICs outside the microcapsules grow and merge into large ice crystals (LICs, double asterisks) at –7 °C (after 20 min annealing) with their boundaries being clearly visible as whitish curves in the phase image (Figure 7A). For the solution

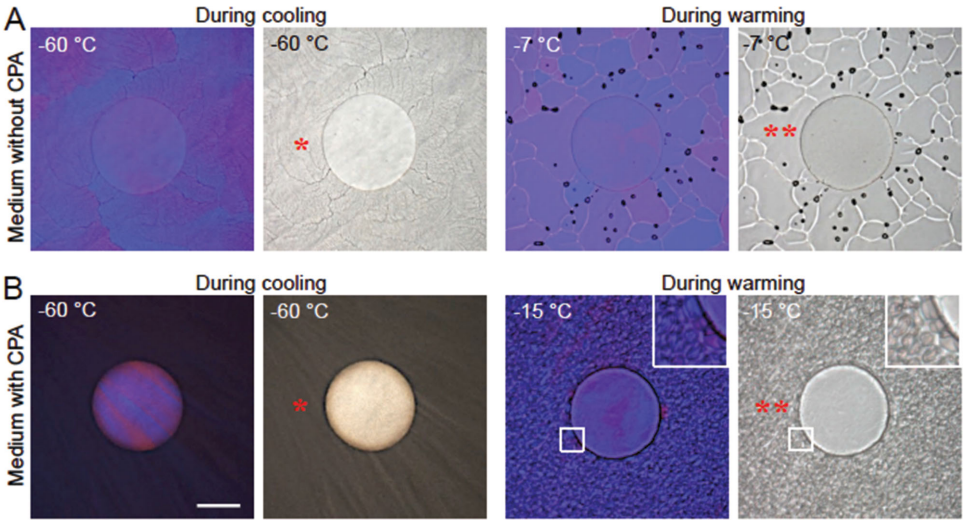

Figure 7. Alginate hydrogel microencapsulation inhibits devitrification during warming. Polarized (color) and phase contrast (grayscale) images at –60 °C at the end of cooling and at –7 and –15 °C during warming with annealing for 20 min for an alginate hydrogel microcapsule in mESC medium without (A) and with (B) CPA (1.5 M PROH and 0.5 M trehalose), respectively. No visible ice formation inside the microcapsule is observable during both cooling and warming while the fine ice crystals (FIC, *) outside the microcapsules in the bulk solution merge into large ice crystals (LIC, **) during warming. Scale bar: 100 μm.

of medium with (penetrating and nonpenetrating) CPAs, the FICs are formed at lower temperature (Figure 2) during cooling and they are finer and darker (more solutes are precipitated from ice crystals compared to the medium without CPA). When warming to –15 °C with 20 min annealing, growth of the FICs into LICs is also evident outside the microcapsule (Figure 7B). The ice growth outside the microcapsule during warming is due to the general tendency of increasing the crystal size to reduce the boundary area and minimize the overall free energy in the system.[11b,20] It is worth noting that the choice at –7 and –15 °C to illustrate ice growth in the bulk medium without and with CPA, respectively, is based on the data shown in Figure 2 for IIF during warming. The temperature for the solution with CPA is lower because the presence of CPA can lower the melting point of the solution.

More importantly, the aforementioned growth of FICs into LICs during warming outside the microcapsules does not occur inside the alginate hydrogel microcapsule at all according to Figure 7: no visible ice formation is observable inside the microcapsule throughout the entire cooling and warming procedure. This confirms the exceptional capability of alginate hydrogel microcapsules in inhibiting devitrification during warming, which should contribute to the high viability and intact functionality of the microencapsulated stem cells post vitrification using QMC or PS as shown in Figures 3, 4, 5, and 6.

3. Discussion

Slow freezing typically has an ice-seeding step to induce ice formation in the extracellular water at a high subzero temperature (usually higher than –10 °C) so that nearly equilibrium freezing of the extracellular water and equilibrium dehydration of cells could be achieved. Such an ice-seeding step is not used for vitrification and the thermodynamics of vitrification is typically nonequilibrium. As a result, for the cryomicroscopy study of IIF during low-CPA vitrification, ice crystals typically form in the extracellular solution at much lower temperatures (≈–20 °C, Figure 2 and Figure S2, Supporting Information) than the thermodynamic equilibrium melting point (usually higher than –10 °C[2b]) of the solutions and they are usually very fine as their growth is hampered by the slow diffusion of water molecules (i.e., diffusion-limited growth) at such deep subzero temperatures.[6a–c,21] Moreover, water transport across the plasma membrane is also stopped because of the low water permeability of the cell plasma membrane at the subzero temperatures,[21,22] leaving an unbalanced osmotic pressure between the intra and extracellular space that tends to dehydrate the cells when possible. However, the fine ice crystals outside the cells can resume their growth during warming to ≈–20 °C (and above) as the mobility of water molecules increases. At the same time, the water permeability of the plasma membrane also increases during warming, allowing water transport across the plasma membrane to release the osmotic imbalance between the intra and extracellular space established during cooling. These nonequilibrium phenomena should also occur during low-CPA vitrification of the nonencapsulated living cells in VSQ with QMC and in VSP with PS since devitrification of the bulk solutions does happen during warming (Figure 4A). These nonequilibrium thermodynamic processes can induce IIF via surface-catalyzed nucleation (SCN) of ice in the cells (**Figure 8**, top row) and dismal cell viability post vitrification/warming ensues (Figures 3B and 4B). It is worth noting that IIF via volume-catalyzed nucleation (VCN) should be minimal here since it usually occurs at temperatures lower than ≈–40 °C.[21]

In the alginate hydrogel microcapsule, by contrast, devitrification during warming is effectively inhibited. As a result, IIF in the microencapsulated cells is minimized during warming (Figure 8, bottom row) and a high cell viability post vitrification ensues (Figures 3, 4, 5, and 6). Of note, although the capability

of alginate hydrogel microencapsulation in inhibiting devitrification may depend on the thermal profile of the device used for vitrification, it was verified over a wide range of warming rate between 100 000 °C min^{-1} (for QMC[10]) and 2000 °C min^{-1} (for PS[7a]) in this study. This is probably because the hydrogel network of the polymer can effectively dampen the movement of water molecules to prevent devitrification from occurring, due to its immense viscosity at subzero temperature and/or the polymer can bind to the surface of invisible nascent ice crystals to inhibit their growth. Further investigations are certainly needed to identify the exact mechanisms that are responsible for the exceptional capability of inhibiting devitrification by the alginate hydrogel microencapsulation.

Although alginate hydrogel microencapsulation is exceptional in inhibiting devitrification during warming, it actually can induce more IIF during cooling at a slow cooling rate (–60 °C min^{-1}, Figure 2 and Figure S2, Supporting Information). This is probably because the invisible ice crystals formed in the microcapsules are much finer (albeit less to give the clearer appearance) than that formed in the bulk solution so that they are easier to trigger IIF via SCN at a subzero temperature higher than –30 °C.[21] Similarly, for nonencapsulated cells during slow cooling, more IIF would occur in the presence of low CPA (Figure 2 and Figure S2, Supporting Information), as the ice crystals in the extracellular solution are finer (albeit extensive to give the darker appearance) with CPA than that without CPA. However, if vitrification of the bulk solution outside (where ice crystals initiate) the microcapsule is achieved via QMC or PS, IIF in the microencapsulated cells could be effectively eliminated (or at least minimized to a nontoxic level) during cooling. This together with the capability of the alginate hydrogel microcapsule in inhibiting devitrification during warming leads to the high survival and intact functional properties of the microencapsulated mESCs and hADSCs post low-CPA vitrification (Figures 3, 4, 5, and 6).

4. Conclusions

In this work, we reveal that during low-CPA vitrification, most of the cells are killed by IIF induced by devitrification in the bulk solution during warming, and alginate hydrogel microencapsulation can effectively inhibit devitrification. As a result, if vitrification of the bulk solution outside the microcapsules could be achieved during cooling, cells microencapsulated in the alginate hydrogel microcapsules could survive well even though devitrification in the bulk solution outside the microcapsule still occurs during warming. Building upon these findings, we achieved low-CPA (2 M PROH as the penetrating CPA) vitrification of mESCs and hADSCs using PS that was thought to be for high-CPA vitrification only. This PS-based low-CPA vitrification technology allows the use of a sample volume that is ≈100 times of that for the QMC-based low-CPA vitrification and eliminates all the disadvantages associated with existing cryopreservation methods. We expect that the finding of the exceptional capability of alginate hydrogel microencapsulation in inhibiting devitrification and the large-volume low-CPA vitrification technology will have a significant impact on the field of cell cryopreservation for banking important cells such as stem cells to meet their ever-increasing demand by the burgeoning cell-based medicine.

5. Experimental Section

Cell Culture: The R1 mESCs (ATCC) were cultured in DMEM supplemented with 15% knockout serum replacement (Invitrogen) containing 1000 U mL^{-1} leukemia inhibitory factor (LIF, Millipore). Feeder layer-free mESCs were cultured in 0.1% gelatin-coated 60 mm culture dishes in humidified 5% CO_2 atmosphere at 37 °C. The primary hADSCs (Lonza) were cultured in hADSC basal medium (Lonza) supplemented with 10% fetal bovine serum (FBS, Invitrogen), 5 mL L-glutamine, and 0.5 mL gentamicin–amphotericin at 37 °C in humidified

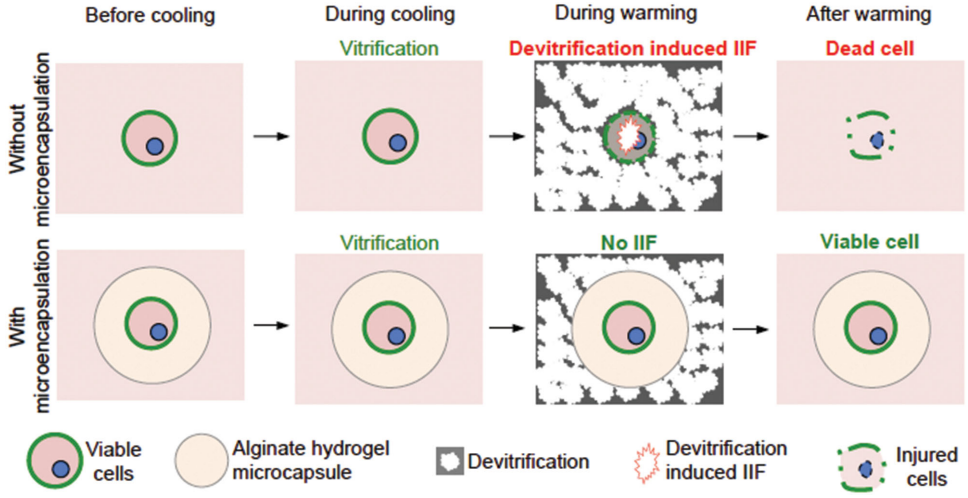

Figure 8. A schematic illustration of the mechanism of augmenting cell vitrification by alginate hydrogel microencapsulation. Although vitrification (i.e., no visible ice formation) could often be achieved during cooling, devitrification of the previously (i.e., during cooling) vitrified solution often occurs during warming. This devitrification could induce significant intracellular ice formation (IIF) in the nonencapsulated cells by surface catalyzed nucleation of ice and cell death ensues (top row). In contrast, devitrification could be effectively inhibited by alginate hydrogel microencapsulation and no significant IIF could occur in the cells encapsulated in the alginate hydrogel microcapsule (bottom row). As a result, the microencapsulated cells could maintain high viability post the entire cooling and warming procedure of vitrification.

5% CO_2 atmosphere. Cells (<passage 5) at ≈80% confluence were detached for passaging and/or further experimental use. All materials for cell culture and other experiments in this study were purchased from Sigma unless specifically mentioned otherwise.

Fabrication of Microfluidic Device: The nonplanar microfluidic devices for cell microencapsulation were fabricated using a multilayer SU-8 fabrication technique detailed elsewhere.[16] After the channel features were molded on a silicon wafer, polydimethylsiloxane (PDMS, Dow Corning) prepolymer and its cross-linking agent (mass ratio: 10:1) were fully mixed and poured onto the wafer to make PDMS slabs (baked at 72 °C for 3 h). The PDMS slabs were peeled off from the wafer, cut into two identical slabs, and aligned under microscope to obtain nonplanar microfluidic device (Figure 1 and Figure S1A, Supporting Information). Finally, the devices were baked at 72 °C for 72 h to make the channel surface hydrophobic for further experimental use.

Microencapsulation of Stem Cells Using Microfluidics: To produce alginate hydrogel microcapsules, the core fluid consisting of 2% (w/v) purified[16c,19] sodium alginate and 0.5 M trehalose either with or without stem cells (cell density 2.5×10^6 cells mL^{-1}) was introduced into the nonplanar microfluidic device via inlet I1 (Figure 1). The presence of trehalose in the core fluid can predehydrate the cells, which may help to suppress intracellular ice formation during cryopreservation.[23] The shell fluid (inlet I2) was prepared by dissolving purified sodium alginate (2%, w/v) in 0.25 M aqueous D-mannitol solution to achieve the isotonic osmolality determined by a micro-Osmometer (Advanced Instruments). The carrier oil emulsion (inlet I3) was made using a method reported previously.[16a] All these solutions were introduced into the microfluidic device using syringe pumps (Harvard Apparatus). The flow rates of inlet I1, I2, and I3 were 75, 75, and 7 mL h^{-1}, respectively. Under these experimental conditions, the cell encapsulation rate was ≈50 cells s^{-1} and all microencapsulation experiments could be completed with 30 min in this study. If desired, the cell concentration and/or microfluidic flow rates could be increased to improve the throughput. Moreover, parallel/multiple microchannels could be fabricated to scale up the microfluidic approach for cell microencapsulation. The microcapsules were collected in cell culture medium and centrifuged at 300 rpm for 3 min to remove carrier oil. They were further gelled in 100×10^{-3} M $CaCl_2$ for 3 min. After the removal of $CaCl_2$ solution by centrifugation at 300 rpm for 3 min, they were resuspended in fresh culture medium and stored at 4 °C for further experiments.

Cryomicroscopy Studies of IIF: Cryomicroscopy studies were performed using a Linkam (Waterfield, UK) FDCS196 freeze-drying stage mounted on an Olympus BX 51 microscope. Real-time images were recorded using a QImaging (Surrey, Canada) Retiga CCD color camera. In each experiment, samples (4 µL) containing cells or microcapsules were loaded into the sample crucible and sandwiched with a coverslip (9 mm in diameter) to obtain clear images during both cooling and warming. The samples were first cooled to −60 °C at 60 °C min^{-1}, held for 2 min, and warmed back at 60 °C min^{-1} to room temperature (24 °C).[21] CPAs were loaded in one step by incubating the cells or cell-laden microcapsules in the cell culture medium with 1.5 M PROH and 0.5 M trehalose for 30 min at 4 °C. For the IIF study of cell-laden microcapsules in mineral oil, the extracapsular solution was replaced with 4 µL of mineral oil.

Cryomicroscopy Study of Inhibiting Devitrification by Alginate Hydrogel Microencapsulation: To investigate the inhibition of devitrification by alginate hydrogel microencapsulation during warming, cryomicroscopy studies were performed to visualize the possible ice formation/growth during both cooling and warming (with annealing) phases of vitrification.[11e,20,24] Briefly, a total of 4 µL mESC medium (either with or without 1.5 M PROH and 0.5 M trehalose) containing alginate hydrogel microcapsules was loaded into the sample crucible of the Linkam cryomicroscopy system and sandwiched with a coverslip (9 mm in diameter) to obtain a thin solution film for taking clear images during both cooling and warming. The samples were first cooled to −60 °C rapidly at 60 °C min^{-1}, held for 2 min, warmed back at 60 °C min^{-1} to either −7 °C (without CPA) or −15 °C (with CPA), and held at the respective temperature for 20 min for annealing to observe ice formation/growth inside and outside the microcapsule under both polarized and phase contrast light microscopy.

Vitrification by QMC and PS: Typical images of the QMC and PS are given in Figure S1B (Supporting Information). The vitrification solution for QMC (VSQ) is the same solution as that used for cryomicroscopy study. The cells in VSQ were loaded into QMC from its stem tip using an aspirator. The vitrification solution for PS (VSP) includes 1.3 M trehalose and 2 M PROH in cell culture medium as the nonpenetrating and penetrating CPAs, respectively. To minimize the contact time to the hypertonic VSP and enhance the diffusion of PROH into cells (VSP is more viscous than VSQ), the encapsulated or nonencapsulated cells were incubated in their medium with 2 M PROH for 30 min at 4 °C, and then transferred into VSP within 1 min before vitrification. For vitrification, the sample-laden QMC or PS was plunged into liquid nitrogen and held for 3 min that is long enough to cool the sample to the temperature of liquid nitrogen.[7d,25] The samples were then warmed back to room temperature by taking the QMC or PS out of liquid nitrogen and plunging them into 1× PBS with 0.2 M trehalose at room temperature. The cell suspension post vitrification was one-step unloaded from the QMC or PS into cell culture medium with 5×10^{-6} M of calcein AM and 5×10^{-6} M of ethidium homodimer (Invitrogen) to stain live and dead cells, respectively. After incubation at 37 °C for 10 min, the live and dead cells stained green and red, respectively, were checked and counted under fluorescence microscopy to determine cell viability.

Functional Tests of mESCs: To further test the functional survival of mESCs, they were released from the alginate microcapsules by liquefying the alginate hydrogel using 75×10^{-3} M tri-sodium citrate post vitrification by PS, washed twice using medium, and put on a mitomycin treated mouse embryonic fibroblast (MEF) feeder layer to culture for 5 d. For qRT-PCR analysis, RNAs were extracted from mESCs using RNeasy plus mini kit (Qiagen) following the manufacturer's instructions. Next, reverse transcription was carried out to generate complementary DNA (cDNA) using the iScript cDNA synthesis kit (Bio-Rad) and GeneAmp 9700 PCR system. The qRT-PCR was conducted with the superfast SYBR Green mix (Bio-Rad) using a Bio-Rad CFX96 real time PCR system. Relative gene expression was calculated using the ΔΔCT method[26] built in the Bio-Rad software. Pluripotency genes including Oct4, Sox2, Nanog, and Klf2 were studied with glyceraldehyde 3-phosphate dehydrogenase (GAPDH) being used as the housekeeping gene (see Table S1, Supporting Information, for information of primers used).

For immunohistochemical staining of two pluripotency marker proteins (Oct4 and SSEA-1), mESCs were fixed in 4% paraformaldehyde, washed three times with 1× PBS, and (for Oct4 staining only) permeabilized with 0.25% Triton X-100. They were then incubated in 3% bovine serum albumin (BSA) in 1× PBST (1× PBS and 0.05% Tween 20) at room temperature for 1 h to block possible nonspecific binding, followed by overnight incubation at 4 °C with primary antibodies (Abcam) targeting Oct4 or SSEA-1. Afterward, they were washed three times and incubated in the dark at room temperature for 45 min with secondary antibodies (Abcam) including DyLight 488 conjugated rabbit IgG and DyLight 550 conjugated mouse IgM for Oct4 and SSEA-1, respectively. All the antibodies were diluted in 3% BSA in 1× PBST. Finally, the cells were washed and their nuclei stained by Hoechst (5×10^{-6} M). To conduct flow cytometry analysis with a BD LSR II Flow Cytometer, mESCs were treated with primary antibodies (Abcam) targeting Oct4 and SSEA-1 and secondary antibodies were DyLight 488 conjugated rabbit IgG and DyLight 550 conjugated mouse IgM for Oct4 and SSEA-1, respectively. Nonstained mESCs were stained in the same way to serve as negative control. The flow cytometry data were further analyzed using the FlowJo software.

For the guided (or directed or coaxed) differentiation of mESCs toward the cardiac lineage, mESCs were first forced to form aggregates by culturing in hanging drop where 1500 cells were suspended in 20 µL of mESC medium as one drop (aggregate) for 2 d. After aggregates were formed, they were plated on gelatin-coated dish with differentiation medium containing DMEM supplemented with 25 ng mL^{-1} BMP-4, 5 ng mL^{-1} bFGF, 100 U mL^{-1} penicillin, and 100 mg mL^{-1} streptomycin for 3 d, followed by DMEM with 20% FBS for two weeks. The

percentage of beating foci in each group was calculated by dividing the maximum number of beating foci with the initial total number of cell aggregates plated. After two weeks, the differentiated cells were harvested for confocal microscopy and flow cytometry studies to examine immunostaining of cTnT (cardiac troponin T, a specific marker of cardiomyocytes) and cTnT positive population, respectively. In brief, cells were processed using the same methods described above for examining pluripotency proteins Oct4 and SSEA-1. They were further incubated with cTnT antibody (Abcam) for 45 min at room temperature, followed by corresponding secondary antibody in the dark. All the samples were resuspended in 0.2 mL ice-cold PBS and studied using a BD LSR-II flow cytometer and the results were further analyzed using FlowJo. Immunostaining of cTnT in the cells was performed by following the instruction of manufacturer (Abcam).

Functional Tests of hADSCs: To test the functional survival of hADSCs post low-CPA vitrification using PS, the cells were released from alginate hydrogel microcapsules in the same way as that for mESCs and further cultured for 3 d before use for functional studies. The expression of stem cell genes was quantified first using qRT-PCR in the same way as that for mESCs. The genes studied and the corresponding primers used are listed in Table S2 (Supporting Information).

For immunostaining of CD44 (positive) and CD31 (negative) receptors, hADSCs at a density of 1×10^5 cells mL^{-1} in 1 mL medium were seeded on type I collagen-coated glass coverslips placed in six-well plate and incubated overnight for attachment onto the coverslips. The samples were then washed with 1× PBS and fixed with 4% paraformaldehyde. The fixed samples were incubated in 3% BSA in 1× PBST at room temperature for 1 h to block potential nonspecific binding, followed by overnight incubation at 4 °C with primary antibody of CD44 or CD31 according to the manufacturer's instructions. Afterward, the samples were washed three times with 1× PBS and incubated in the dark at room temperature for 1 h with secondary antibodies diluted in 3% BSA in 1× PBST (1:50 dilution). The samples were then washed and stained for nuclei using Hoechst 33342 (5×10^{-6} M) for further microscopic examination.

To quantify the expressions of CD44 and CD31 receptors by flow cytometry, the detached hADSCs were washed with 1× PBS and stained with CD44-FITC (Invitrogen) and CD31-FITC (Abcam) antibodies separately according to the manufacturers' instructions. The stained samples were analyzed using a BD LSR-II Flow cytometer together with FlowJo software.

To study the multilineage potential of hADSCs, experiments on guided adipogenic, osteogenic, and chondrogenic differentiation were conducted. For adipogenic differentiation, a total of 2×10^5 cells were seeded in 2 mL of the hADSC medium and the medium was changed every 2 d until the cell became confluent. Afterward, three cycles of induction/maintenance were performed to induce adipogenic differentiation. Each cycle consisted of culturing the hADSCs in adipogenic induction medium (Lonza) for 3 d, followed by 1 d culture in adipogenic maintenance medium (Lonza). After three complete cycles of induction/maintenance, the cells were cultured for 7 d in adipogenic maintenance medium that was changed every 2 d. On the last day of differentiation, the adipogenic maintenance medium was removed and the cells were rinsed with 1× PBS and fixed for 30 min with 2 mL of 4% paraformaldehyde solution. The fixed cells were rinsed twice with 1× PBS and stained with 1 mL of oil red O working solution (Cyagen, after 3:2 dilution using distilled water and filtering with 20–25 μm filter paper) for 30 min. The cells were then rinsed three times with 1× PBS for further analysis using a Nikon 80i microscope equipped with a QImaging Retiga CCD color camera.

For osteogenic differentiation, a total of 3×10^4 cells were seeded in 2 mL medium in 0.1% collagen coated six-well plate to prevent cells from peeling off during differentiation. After culturing for 24 h in the hADSC culture medium, the culture medium was replaced with osteogenic induction medium (Lonza) that was changed every 2 d for three weeks. The osteogenic differentiation medium was then removed and the cells were rinsed with 1× PBS and fixed for 30 min in 2 mL 4% paraformaldehyde solution. The fixed cells were rinsed with 1× PBS twice and stained in 1 mL alizarin red S working solution (Cyagen) for 3 min. The stained cells were rinsed three times with 1× PBS for further analysis using the Nikon 80i microscope.

For chondrogenic differentiation, a total of 2.5×10^5 hADSCs were washed twice with 1 mL incomplete chondrogenic induction medium (Lonza). The cells were then resuspended in 0.5 mL of complete chondrogenic induction medium (Lonza) at 5×10^5 cells mL^{-1}. Afterward, the cell suspension was transferred into 15 mL polypropylene culture tubes and centrifuged at 150×g for 5 min at room temperature. The caps of the tubes were then loosened to allow gas exchange and the cell pellets in the tubes were incubated at 37 °C in a humidified atmosphere with 5% CO_2 for 21 d. The medium was changed every 2–3 d. Afterward, the pellets were harvested and fixed with 4% paraformaldehyde. The fixed pellets were then embedded with paraffin and stained with Alcian blue assay (Cyagen). The stained slides were then analyzed using the Nikon 80i microscope.

Imaging: Videos of the generation and transportation of microcapsules in microchannels were recorded using a fast-speed CCD camera (AxioCam HSm) equipped on a Zeiss Axio Observer.Z1 microscope under bright field with 2.5× objective. To check cell viability and pluripotency post vitrification, both phase contrast (or differential interference contrast/DIC) and fluorescence images were taken using a Zeiss AxioCam MR3 CCD camera equipped on the same microscope.

Data Analysis: The data for cumulative percentage of IIF are presented by pooling together the data from at least three independent experiments because IIF generally does not occur at the same temperatures in different experiments. The percentage of area stained by ORO, ARS, and AB in hADSC differentiation studies was calculated using Matlab R2012a (MathWorks). All other data are reported as mean ± standard deviation (SD) from at least three independent runs. The *p*-value for comparing two groups was determined by Student's two-tailed *t*-test in Microsoft Excel to assess statistical significance and a *p*-value less than 0.05 is taken as statistically significant.

Supporting Information

Supporting Information is available from the Wiley Online Library or from the author.

Acknowledgements

H.H. and J.K.C. contributed equally to this work. This work was partially supported by grants from NSF (CBET-1154965) and NIH (R01EB012108).

Received: July 22, 2015
Revised: September 8, 2015
Published online: October 15, 2015

[1] a) R. Langer, J. P. Vacanti, *Science* **1993**, *260*, 920; b) J. Gearhart, *Science* **1998**, *282*, 1061; c) M. F. Pittenger, A. M. Mackay, S. C. Beck, R. K. Jaiswal, R. Douglas, J. D. Mosca, M. A. Moorman, D. W. Simonetti, S. Craig, D. R. Marshak, *Science* **1999**, *284*, 143.

[2] a) X. He, in *Methodological Advances in the Culture, Manipulation and Utilization of Embryonic Stem Cells for Basic and Practical Applications* (Ed: C. Atwood), InTech Publisher, Vienna, Austria **2011**, p. 113; b) X. He, *Open Biomed. Eng. J.* **2011**, *5*, 47; c) H. Niwa, J. Miyazaki, A. G. Smith, *Nat. Genet.* **2000**, *24*, 372.

[3] a) P. Mazur, *Science* **1970**, *168*, 939; b) M. Toner, E. G. Cravalho, M. Karel, *J. Appl. Phys.* **1990**, *67*, 1582.

[4] a) M. Toner, in *Advances in Low-Temperature Biology* Vol. *2* (Ed: P. L. Steponkus), Jai Press Ltd., London **1993**, p. 1; b) A. Fowler, M. Toner, *Ann. N. Y. Acad. Sci.* **2005**, *1066*, 119.

[5] a) P. Mazur, *Am. J. Physiol.* **1984**, *247*, C125; b) K. R. Diller, *J. Biomech. Eng.* **2005**, *127*, 67.
[6] a) J. O. M. Karlsson, E. G. Cravalho, M. Toner, *J. Appl. Phys.* **1994**, *75*, 4442; b) G. Yang, A. Zhang, L. X. Xu, X. He, *J. Appl. Phys.* **2009**, *105*, 114701; c) G. Zhao, H. Takamatsu, X. M. He, *J. Appl. Phys.* **2014**, *115*, 144701; d) G. M. Fahy, B. Wowk, J. Wu, S. Paynter, *Cryobiology* **2004**, *48*, 22.
[7] a) W. F. Rall, G. M. Fahy, *Nature* **1985**, *313*, 573; b) J. O. Karlsson, M. Toner, *Biomaterials* **1996**, *17*, 243; c) B. C. Heng, L. L. Kuleshova, S. M. Bested, H. Liu, T. Cao, *Biotechnol. Appl. Biochem.* **2005**, *41*, 97; d) X. He, E. Y. Park, A. Fowler, M. L. Yarmush, M. Toner, *Cryobiology* **2008**, *56*, 223.
[8] a) S. Yavin, A. Arav, *Theriogenology* **2007**, *67*, 81; b) D. K. Gardner, C. B. Sheehan, L. Rienzi, M. Katz-Jaffe, M. G. Larman, *Theriogenology* **2007**, *67*, 64; c) G. Vajta, Z. P. Nagy, *Reprod. BioMed. Online* **2006**, *12*, 779; d) W. Zhang, G. Yang, A. Zhang, L. X. Xu, X. He, *Biomed. Microdevices* **2010**, *12*, 89; e) H. J. Lee, H. Elmoazzen, D. Wright, J. Biggers, B. R. Rueda, Y. S. Heo, M. Toner, T. L. Toth, *Reprod. BioMed. Online* **2010**, *20*, 201.
[9] B. Wowk, E. Leitl, C. M. Rasch, N. Mesbah-Karimi, S. B. Harris, G. M. Fahy, *Cryobiology* **2000**, *40*, 228.
[10] R. Risco, H. Elmoazzen, M. Doughty, X. He, M. Toner, *Cryobiology* **2007**, *55*, 222.
[11] a) B. M. Eriksson, H. Rodriguez-Martinez, *Anim. Reprod. Sci.* **2000**, *63*, 205; b) C. A. Knight, D. Wen, R. A. Laursen, *Cryobiology* **1995**, *32*, 23; c) F. Dumont, P. A. Marechal, P. Gervais, *Appl. Environ. Microbiol.* **2006**, *72*, 1330; d) J. L. Chaytor, J. M. Tokarew, L. K. Wu, M. Leclere, R. Y. Tam, C. J. Capicciotti, L. Guolla, E. von Moos, C. S. Findlay, D. S. Allan, R. N. Ben, *Glycobiology* **2012**, *22*, 123; e) R. C. Deller, M. Vatish, D. A. Mitchell, M. I. Gibson, *Nat. Commun.* **2014**, *5*, 3244; f) S. Seki, B. Jin, P. Mazur, *Cryobiology* **2014**, *68*, 71; g) S. Seki, P. Mazur, *PLoS One* **2012**, *7*, e36058; h) B. Jin, F. W. Kleinhans, P. Mazur, *Cryobiology* **2014**, *68*, 419; i) B. Jin, P. Mazur, *Sci. Rep.* **2015**, *5*, 9271.
[12] a) M. Serra, C. Correia, R. Malpique, C. Brito, J. Jensen, P. Bjorquist, M. J. Carrondo, P. M. Alves, *PLoS One* **2011**, *6*, e23212; b) R. Malpique, L. M. Osorio, D. S. Ferreira, F. Ehrhart, C. Brito, H. Zimmermann, P. M. Alves, *Tissue Eng., Part C* **2010**, *16*, 965.
[13] J. Mumaw, E. T. Jordan, C. Sonnet, R. M. Olabisi, E. A. Olmsted-Davis, A. R. Davis, J. F. Peroni, J. L. West, F. West, Y. Lu, S. L. Stice, *Int. J. Biomater.* **2012**, *2012*, 861794.
[14] A. S. Utada, A. Fernandez-Nieves, H. A. Stone, D. A. Weitz, *Phys. Rev. Lett.* **2007**, *99*, 094502.
[15] T. C. T. G. Mason, *Phys. Fluids* **2008**, *20*, 11.
[16] a) H. Huang, X. He, *Appl. Phys. Lett.* **2014**, *105*, 143704; b) P. Agarwal, S. Zhao, P. Bielecki, W. Rao, J. K. Choi, Y. Zhao, J. Yu, W. Zhang, X. He, *Lab Chip* **2013**, *13*, 4525; c) J. K. Choi, P. Agarwal, H. Huang, S. Zhao, X. He, *Biomaterials* **2014**, *35*, 5122.
[17] J. Happel, H. Brenner, *Low Reynolds Number Hydrodynamics: With Special Applications to Particulate Media*, Kluwer Boston, Boston, MA, USA **1983**.
[18] G. Yang, A. Zhang, L. X. Xu, *Cryobiology* **2011**, *63*, 38.
[19] S. Zhao, P. Agarwal, W. Rao, H. Huang, R. Zhang, Z. Liu, J. Yu, N. Weisleder, W. Zhang, X. He, *Integr. Biol.* **2014**, *6*, 874.
[20] D. A. Wharton, P. W. Wilson, J. S. Mutch, C. J. Marshall, M. Lim, *CryoLetters* **2007**, *28*, 61.
[21] G. Yang, M. Veres, G. Szalai, A. Zhang, L. X. Xu, X. He, *Ann. Biomed. Eng.* **2011**, *39*, 580.
[22] R. V. Devireddy, D. Raha, J. C. Bischof, *Cryobiology* **1998**, *36*, 124.
[23] W. Rao, H. Huang, H. Wang, S. Zhao, J. Dumbleton, G. Zhao, X. He, *ACS Appl. Mater. Interfaces* **2015**, *7*, 5017.
[24] a) M. I. Gibson, C. A. Barker, S. G. Spain, L. Albertin, N. R. Cameron, *Biomacromolecules* **2009**, *10*, 328; b) R. C. Deller, T. Congdon, M. A. Sahid, M. Morgan, M. Vatish, D. A. Mitchell, R. Notmana, M. I. Gibsona, *Biomater. Sci.* **2013**, *1*, 478.
[25] a) J. K. Choi, H. Huang, X. He, *Cryobiology* **2015**, *70*, 269; b) J. K. Choi, T. Yue, H. Huang, G. Zhao, M. Zhang, X. He, *Cryobiology* **2015**, DOI: 10.1016/j.cryobiol.2015.08.012.
[26] W. Zhang, S. Zhao, W. Rao, J. Snyder, J. K. Choi, J. Wang, I. A. Khan, N. B. Saleh, P. J. Mohler, J. Yu, T. J. Hund, C. Tang, X. He, *J. Mater. Chem. B* **2013**, *1*, 1002.